

Chapter 1

Experimental results

Noise limitations

Lab measurements

Temperature and radiation limitations

Transient current technique

Charge - before and after irradiation

compare with RD42 results

Generation of trapping centres, reference KIT, Marok, Harris

IIa

This chapter contains the measurement results of data taken with diamond sensors. The description of measurement setup (section 1.1) and the experimental technique (section ??) is followed by discussion of limitations in sections 1.3, 1.4 and 1.6. The aim of the chapter is to compare the experimentally acquired data with the theory from the previous chapter.

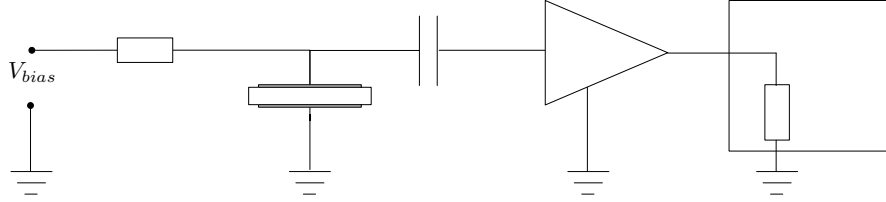


Figure 1.1: Diagram of a diamond detector readout chain.

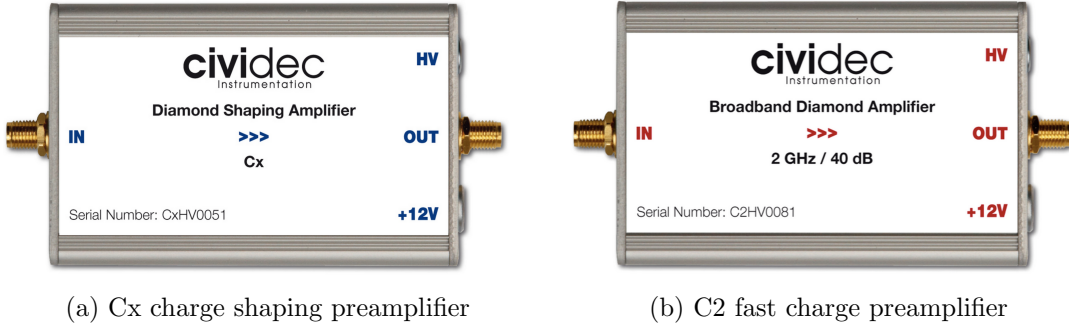


Figure 1.2: Thermal neutron measurement setup

1.1 Measurement setup

The measurement chain consists of three main parts: a diamond sensor, a signal preamplifier and a readout device, as seen in diagram 1.1.

The signals propagating along the analogue chain are fast and with low amplitudes, which gives rise to importance of RF shielding. For instance, the sensor carrier has to be RF-tight to shield from external interferences. Also, the connection between the carrier and the preamplifier has to be as short as possible to avoid capacitive signal losses in the transmission line. Finally, the system needs to be grounded properly.

1.1.1 Preamplifiers

Two preamplifiers were used for the measurements, both embedded in an RF-tight aluminium box to reduce the noise pickup. Both have an AC coupled input and a $50\ \Omega$ output.

CIVIDEC C2 is a fast current preamplifier with a 2 GHz bandwidth limit. It is used for TCT measurements because of its fast response and a good SNR.

CIVIDEC Cx is a charge shaping amplifier. Its high SNR (low noise of 400 electrons and gain of 8.2 mV/fC) makes it a good choice for spectroscopic measurements with diamond sensors.

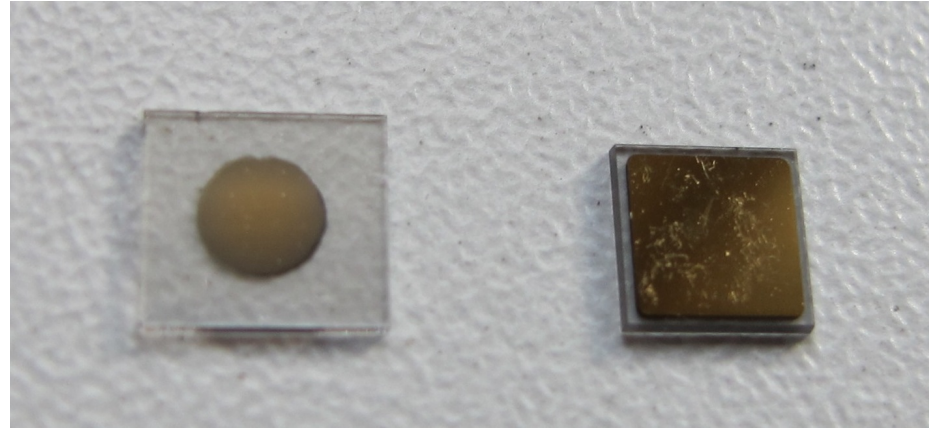


Figure 1.3: Two scCVD diamond samples: A IIa 1scdhq (size $5.3 \times 5.6 \times 0.460 \text{ mm}^3$) and a E6 S37 (dimensions $4.7 \times 4.7 \times 0.548 \text{ mm}^3$)

Diamond samples

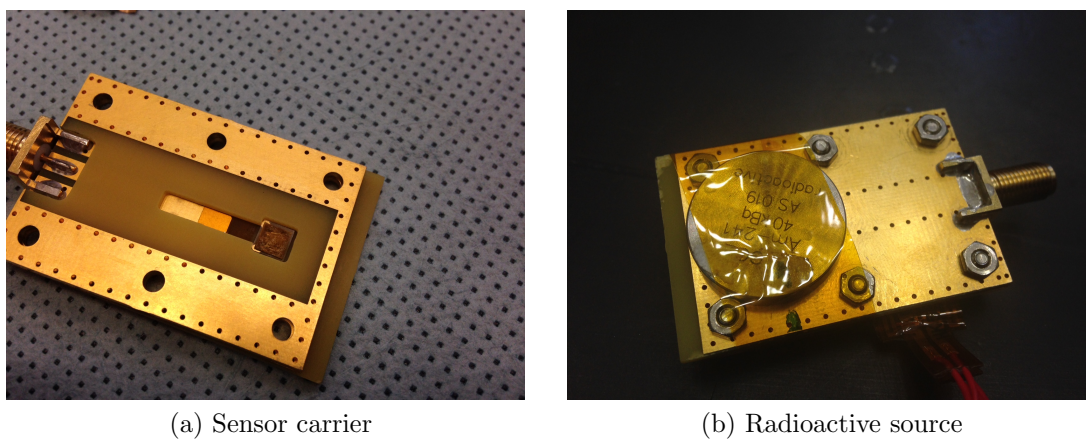
Table 1.1: Diamond sensor samples used

Name	Producer	Dimensions (x, y) [mm ²]	Thickness [μm]	Irradiated
S37	E6	4.7×4.7	548	no
S50	E6	4.7×4.7	537	no
S52	E6	4.7×4.7	515	$1 \times 10^{14} \text{ p/cm}^{-2}$
S79	E6	4.7×4.7	529	$3.63 \times 10^{14} \text{ p/cm}^{-2}$
ELSC	E6	4.7×4.7	491	no
1scdhq	IIa	5.6×5.3	460	no

Readout device

Oscilloscopes are the most versatile analogue signal readout devices - fast to set up and reliable. It is important, though, to choose an oscilloscope with high enough bandwidth, especially for the fast current preamplifier signals. The choice for this setup was a 1 GHz and a 2 GHz option from the LeCroy WaveRunner family.

1.1.2 Cryogenic setup



(a) Sensor carrier

(b) Radioactive source

Figure 1.4: Positioning of the α -source on top of the sensor carrier

1.2 Particle and photon pulses and spectra

1.3 Noise limitations

TO DO: Take 8 runs with the 2GHz oscilloscope while increasing the noise.

Noise is a major limiting factor in particle detection. It defines the minimum measurable particle energy. It is hence important to

1.4 Temperature limitations

A test was carried out to evaluate the effect of temperature changes on the output signal of the diamond sensors. A cryostat filled with liquid helium was used to cool down the sensor during the measurement process. Current signal response to α -particles was measured at 18 temperature points between 4 K and 295 K (room temperature - RT). At every temperature point, a set of 300 pulses was read out at various bias voltages. Resulting data showed that the charge collection is stable down to 150 K, where it starts decreasing and stabilises again at about one third of the initial value at 75 K. This behaviour was first measured and discussed by H. Jansen in [?].

1.4.1 Temperature-variant TCT

The band gap energy in diamond equals to $E_g = 5.5$ eV while the average energy to produce an electron-hole pair is $E_{e-h} = 13.25$ eV. This means there is excessive energy deposited in the diamond bulk. The impinging α -particle stops within ~ 10 μm of the bulk, transferring all its energy to the lattice. A part of this energy, approximately 40 %, directly ionises the carbon atoms, creating free electron-hole pairs. The remaining energy, however, is converted into lattice vibrations (phonons [?]). This effectively means that the lattice within the ionisation volume (approximately ~ 10 $\mu\text{m} \times \sim 2$ nm in size) is briefly heated up. The hot plasma then cools down to the temperature of the surrounding material by heat dissipation, (i.e. phonon transport).

The positively charged hole and negatively charged electron in the hole attract each other via the Coulomb force and may undergo a bonding process during which a phonon is emitted. That phonon is referred to as *exciton* [?]. The electron is pushed to a so-called exciton energy band, which is 80 mV under the conduction band. At higher temperatures, the lattice provides enough energy to excite the electron from the exciton state back to the valence band (so-called exciton recombination). At lower temperatures, however, the exciton lifetime increases, which means that it will take a longer time for the electrons to get re-excited to the valence band. The re-excitation lifetime at room temperature is ~ 30 ps, increasing to ~ 150 μs at 50 K.

Temperature-variant pulse shapes

Three sCVD diamond samples were tested at the range of temperatures. Resulting averaged pulses are shown in a set of figures 1.5. Some conclusions can be drawn by observing their shape. First, the pulses from hole collection are shorter than those from the electron collection, proving that holes indeed travel faster in diamond. Second, the pulse shapes change with decreasing temperature. In particular, the pulse time gets shorter, hinting at the faster carrier drift velocity v_{drift} . Third, between 150 K and 75 K there is a significant change in shape - the time constant of the rising

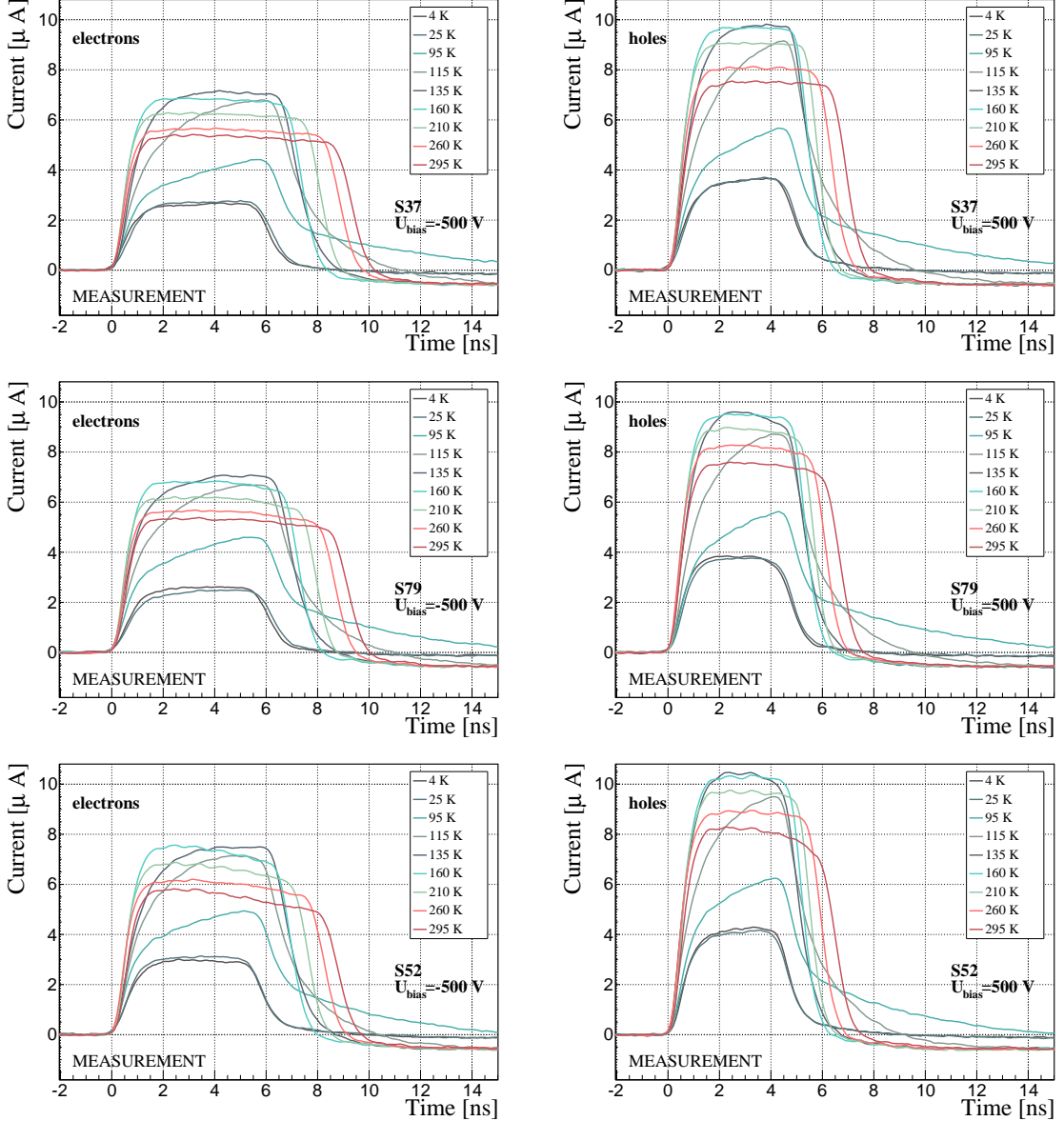


Figure 1.5: Several data points between 4 K and 295 K at a bias voltage of ± 500 V

edge increases significantly and the pulse area decreases. From 75 K down to 4 K there is no significant change. Last, the top of the pulse at the S52 is not flat, which hints on charge loss along the way. This could be due to impurities in the diamond bulk, which act as charge traps. All in all, the pulse shape changes significantly with temperature, which is predicted by H. Jansen's model.

Figure 1.6 shows the pulses at different bias voltages at a fixed temperature. Again it is evident that the pulse width decreases with increasing bias voltage.

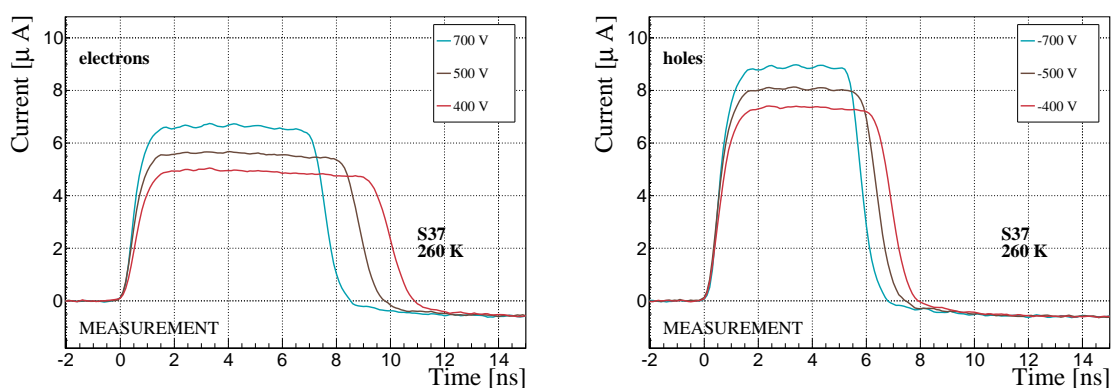


Figure 1.6: Varied bias voltage at a fixed temperature

1.5 Radiation limitations

Exposure to ionising radiation degrades sensors. It introduces so-called charge traps in the sensor material. The electrons and holes created by the impinging particle get trapped in these traps, decreasing the induced current on the electrodes. This yields a lower integrated charge in an irradiated sensor than that in a non-irradiated one. Charge collection efficiency is therefore correlated with the level of irradiation. In semiconductors, it follows an inverse exponential curve ?????

1.5.1 Quantifying radiation damage in diamonds

The last few decades have seen extensive efforts put into understanding and quantifying radiation damage in semiconductors. This varies with the type of radiation (particles or photons) and its energy. There are models existing that try to explain the impact of irradiation and to provide *hardness factors* to compare the radiation damage between different particles. The standard way is to convert the damage into *neutron equivalent*. Some models have been extensively verified with simulations and experimentally. In these experiments charge collection in sensors is measured before and after irradiation. This procedure is repeated several times, with a measurement point taken after every irradiation. When a set of measurements of charge collection is plotted against the radiation dose received by a specific particle at a specific , a damage factor k_λ can be extracted. Damage factors across a range of energies and types of particles (photons) have to be measured to properly quantify the damage in the sensors. They are then compared against the simulations to verify that the experimental observations are in line with the theory.

Radiation damage in silicon, for instance, is well understood and explained. Silicon sensor is relatively cheap and widespread, which facilitated the irradiation experiments. Diamond, however, is an expensive material and the technology is relatively new as compared to silicon. Therefore not many institutes are carrying out diamond irradiation studies. To join the efforts, a collaboration called RD42 was formed. It gathers the experimental data from diamond irradiation studies. Unlike with silicon, the experimental results so far show no significant correlation with the NIEL (non-ionising energy loss) model [?], which correlates detector efficiency with the *number of lattice displacements*. Therefore an alternative model was proposed by Karlsruhe Institute of Technology [?], correlating the diamond efficiency with *displacements per atom* (DPA) in the bulk. Figure 1.7 shows the DPA model for a range of energies of proton, pion and neutron irradiation in diamond. It has been normalised to damage in 24 GeV protons. According to the plot, a 300 MeV pion beam damages the diamond bulk twice as much as a 24 GeV proton beam.

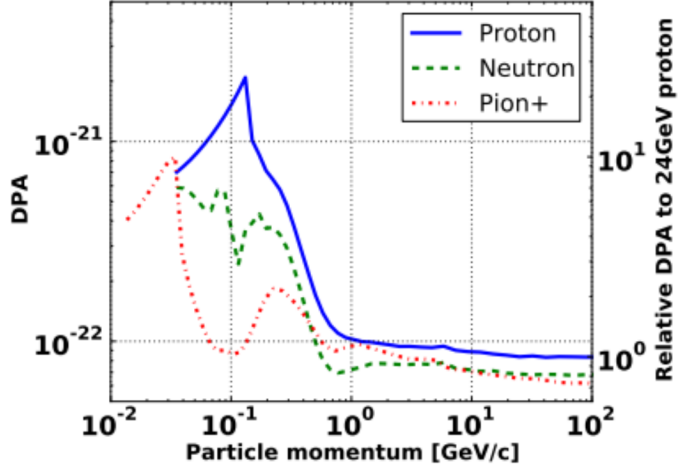


Figure 1.7: Diamond radiation damage - a model based on displacements per atom.
Courtesy Karlsruhe Institute of Technology [] PLACEHOLDER

Pion irradiation

Paul Scherrer Institute (PSI) is the largest research institute for material sciences in Switzerland. Among other they also carry out irradiation campaigns. Their 300 MeV/c (kinetic energy 191.31 MeV) pion beam with a flux of up to $1.5 \times 10^{14} \text{ pions cm}^{-2} \text{ day}^{-1}$. Due to the uncertainty on the hardness factor, the equivalent fluences have an error of $\pm 20\%$.

Two diamond samples, S52 and S79, were exposed to the pion beam in the 2014 PSI irradiation campaign; S52 to $1 \times 10^{14} \text{ pions cm}^{-2}$ and S79 to $3.63 \times 10^{14} \text{ pions cm}^{-2}$. During the process, the golden electrodes got slightly activated, but the activation decayed in two weeks.

Charge collection distance

Three diamonds – non-irradiated S37 and irradiated S52 and S79 – were exposed to a 120 GeV test beam before and after irradiation to estimate the charge collection distance (CCD) and its decrease after irradiation. The samples were "pumped" prior to data taking using a ${}_{90}\text{Sr}$ radioactive source. Data were then taken at a range of bias voltages from 30 V to 500 V, yielding up to 1 V/ μm electrical field in the bulk. Every data point contained approximately 5×10^4 measured particles. The charge deposited by the particles was measured using a CIVIDEC Cx charge preamplifier. As expected, the integrated amplitude spectrum followed a landau distribution, as seen in figure 1.10. Its most probable value (MPV) was used to calculate the most probable collected charge Q_i :

$$Q_i [e] = Q_i [fC] \cdot 6.241 \times 10^{18} = \frac{\text{MPV} [\text{mV}]}{A [\text{mV}/fC]} \cdot 6.241 \times 10^{18} \quad (1.1)$$

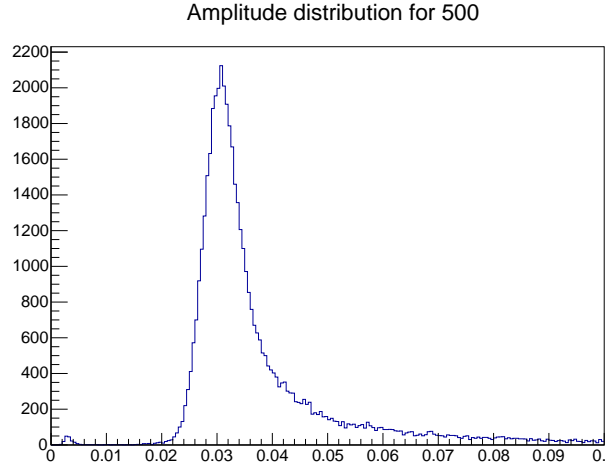


Figure 1.8: An example of a landau distribution acquired by S37 at 500 V bias voltage
PLACEHOLDER

where A is the preamplifier gain factor. The CCD was then calculated using the average number of electron-hole pairs produced per micrometer in diamond $\delta_d = 36 e^- h \mu m^{-1}$:

$$CCD = \frac{Q_i}{\delta_d} \quad (1.2)$$

The resulting CCD for the three measured samples at bias voltages ranging from $0.2\text{--}1.0 V \mu m^{-1}$ is shown in figure 1.9a. S37 exhibits full collection distance already at $0.4 V \mu m^{-1}$ whereas the irradiated samples have a more gentle increase of CCD with increasing bias voltage. It is evident that at $1 V \mu m^{-1}$ the maximum CCD has not been reached in the case of S79 and S52.

Irradiation damage factor

The irradiation damage factor k is a way to quantify irradiation damage of a specific particle at a specific energy. Via this factor different types of irradiation can be compared. It is obtained experimentally by measuring the CCD of a number of samples at various irradiation steps and fitting the function 1.4 to the data. λ is the measured CCD, λ_0 is the CCD of a non-irradiated sample and Φ the radiation dose.

$$\frac{1}{\lambda} = \frac{1}{\lambda_0} + \frac{k}{\Phi} \quad (1.3)$$

$$\lambda = \frac{\lambda_0}{k\lambda_0\Phi + 1} \quad (1.4)$$

The data points with the maximum CCD obtained in the test beam measurements were plotted against radiation dose received (see figure 1.9b). Function 1.4 was fitted

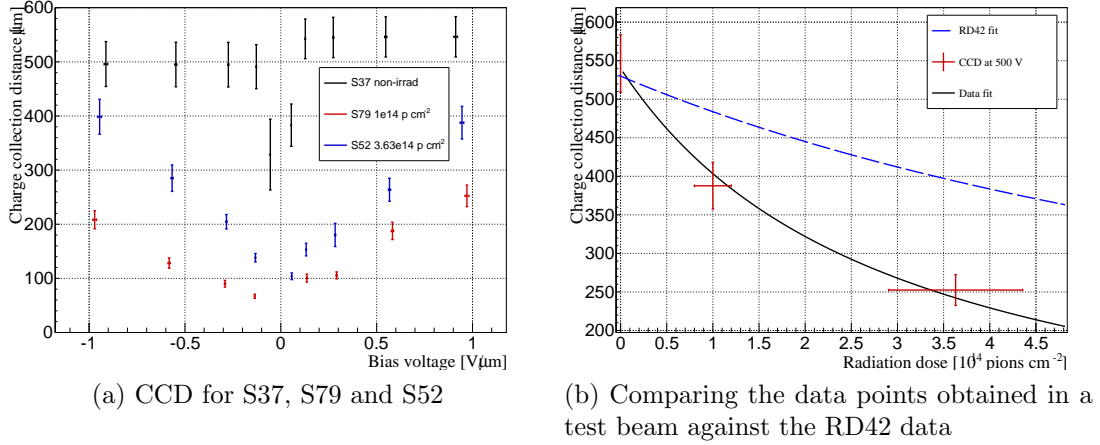


Figure 1.9: The charge collection distance at 500 V bias voltage for the three diamond samples was compared to the RD42 data for pion irradiation. The data points are not in accordance with the model.

Figure 1.10: Change of the pulse shape with time. PLACEHOLDER

to the data points and a damage factor $k = 6.2 \times 10^{-18}$ was obtained. This is three times higher than the damage factor obtained by RD42. A possible cause is that the irradiated samples did not yet have a full charge collection at $1 \text{ V } \mu\text{m}^{-1}$.

1.5.2 TCT at room temperature

Long-term charge collection stability

TO-DO: Ramp up to 500 V, take 100 samples every 5 minutes.

The three samples were tested for a long term stability of the current pulse shapes.

Charge collection hysteresis

1.5.3 Temperature-variant TCT

The irradiated samples were put in the cryostat, which was cooled down to 4.2 K using liquid helium. TCT data were then taken at a range of bias voltages at temperature points ranging between 4.2 K and room temperature (RT). The results showed that irradiation causes forming of charge traps in the bulk.¹

TO-DO: get the Tau and plot it against T. TO-DO: plot the drift time against square voltage.

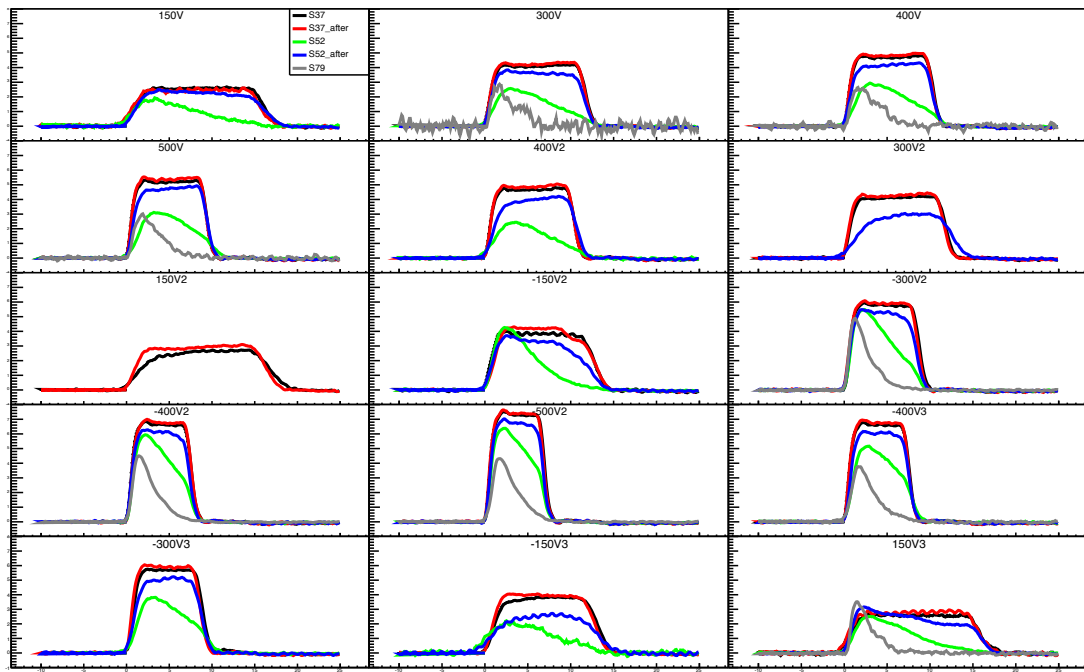


Figure 1.11: S37 non-irrad; S52 $1 \times 10^{14} p \text{ cm}^{-2}$ non-pumped, pumped; S79 $3.63 \times 10^{14} p \text{ cm}^{-2}$ non-pumped, pumped PLACEHOLDER

1.6 Conclusion

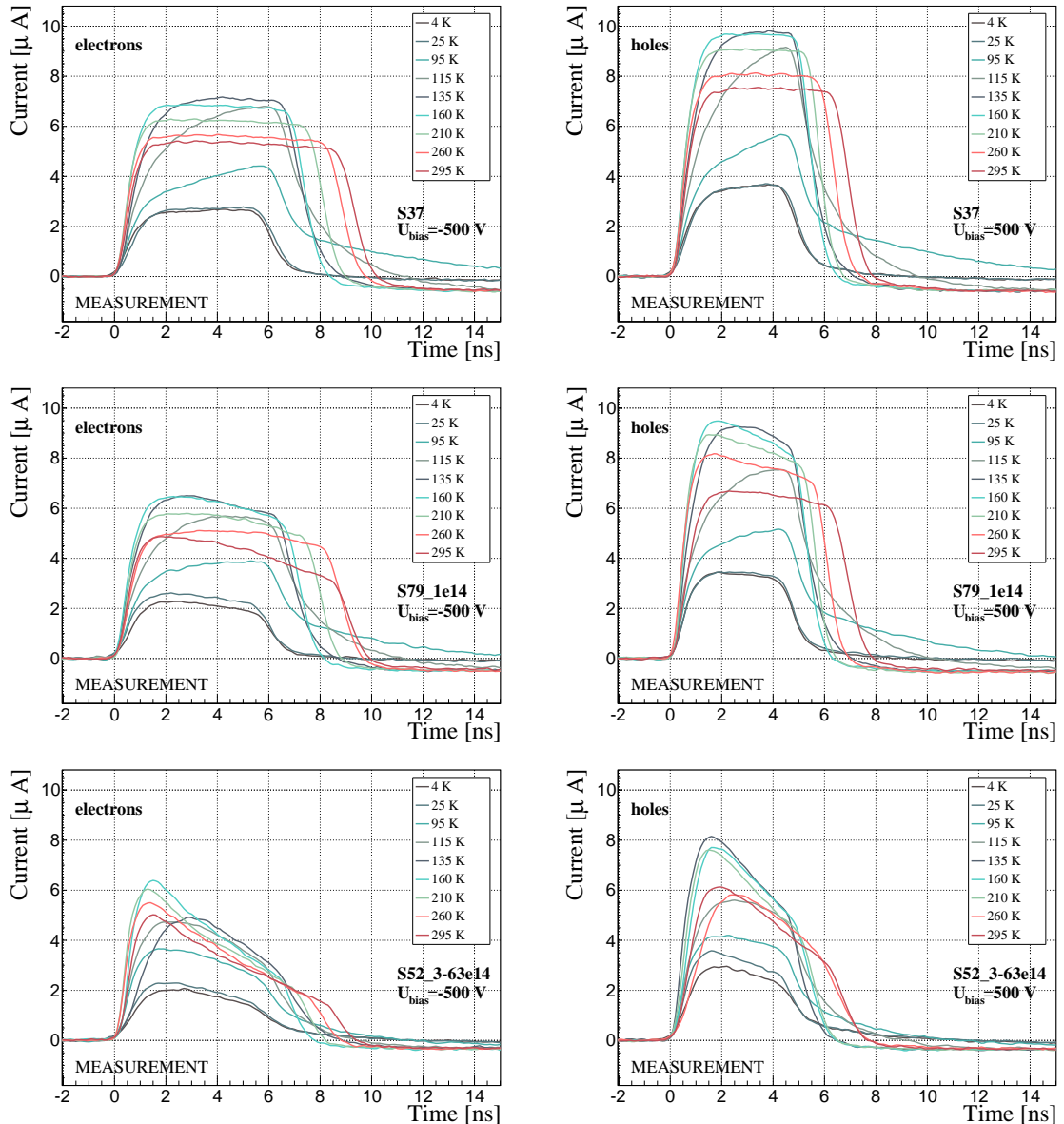


Figure 1.12: Several data points between 4 K and 295 K at a bias voltage of ± 500 V